Stability against Overturning of Curved Continuous Box-Girder Bridges with Single Column Piers

Guohua Song[1, *], Delu Che[2], Minghui Li[3]

[1]School of Civil Engineering, Zhengzhou University, Zhengzhou 450001, China
[2]School of Civil Engineering, Tongji University, Shanghai 200092, China
[3]The First Construction Co., LTD of China Construction First Group, Shanghai 20100, China

*Corresponding author e-mail: guohuasong_309@163.com

Abstract. This paper introduces the factor of stability against overturning (FSO) for curved bridges, and examines the influence of curvature radius and bearing eccentricity on FSO under self-weight and vehicle loads as well as other important parameters. The results show that FSO variation rules are indeed affected by curvature radius and bearing eccentricity. Lane loads are identified as crucial parameters in the overturning resistance of curved bridges. Bearing eccentricity influences the inner side and outer side reactions of abutment bearings, but the optimal bearing eccentricity can ensure uniform torque distribution; said optimal eccentricity is expressed as a function of curvature radius. FSO increases as bearing eccentricity increases, but decreases first followed by a later increase as curvature radius increases. The FSO curve with curvature radius is concave. There exist specific curvature radii near the lowest point in the FSO curve which must be avoided in the design stage to meet necessary safety demands. When curvature radius exceeds 500 m, the FSO converges on an identical curve which can be expressed as a function of curvature radius.

1. Introduction

Single column piers lend important advantages to bridges including simple substructure, facile construction, and effective transparency to the horizon, making them popular in many overpass bridges and viaducts across the globe. Many previous researchers have explored curved bridges, but typically emphasize calculation at ultimate limit states and service limit states, such as bending and shear resistances [1, 2]. There has been relatively little research on the action of accidental eccentric loads.

Bridges with single column piers are prone to overturning accidents due to their simple boundary conditions [3, 4]. These accidents are typically characterized by vehicles deviating from their normal lanes. On a small or light curved ramp bridge, overturning moment resistance may be suddenly unable to balance out the overturning moment caused by industrial trucks, especially in thick traffic or under heavier loads [5-9]. When bearings separate, the boundary conditions of the superstructure fail and the girder is likely to overturn [10-13].

Curved bridges are more complex than straight bridges both mechanically and in terms of their detailed design. There have been few studies on their stability against overturning or the precise mechanisms and occurrence of overturning accidents on curved bridges, however. Methods for checking

the stability against overturning are rarely explicitly stated either at home [14] or abroad [15, 16]; in most cases only simple captions are given. In China, even the current code JTG D60-2015 [17] has neither specific regulations nor guiding methodology for this purpose, which leaves curved bridges susceptible to poor overturning resistance at the design stage and to overturning accidents at the service stage. There is urgent demand for new techniques for assessing stability against overturning in curved bridges [18, 19].

Many factors influence stability against overturning, including curvature radius, bearing eccentricity, temperature effect, torsional pier spacing, foundation settlement, and superstructure dimensions [2, 11-13, 20, 21]. One parameter cannot account for the overall stability against overturning. The present study was conducted to analyze the influence of curvature radius and bearing eccentricity on stability against overturning in curved bridges with single column piers per the novel concept factor of stability against overturning (FSO). An early draft of Chinese regulation JTG D62-2012 (exposure draft) [22] describes the term FSO for verifying bridge safety against overturning. G. H. Song et al [23] have given the method of choosing the overturning axis. The paper will research on the stability against overturning of curved continuous box-girder bridges with single column piers.

2. FSO concept in detail

An early draft of Chinese regulation JTG D62-2012 (exposure draft) [22] describes the term FSO for verifying bridge safety against overturning. The overturning resistance of a given bridge superstructure satisfies the following formula:

$$k_{\mathrm{qf}} = \frac{S_{\mathrm{bk}}}{\mathrm{S}_{\mathrm{sk}}} \geq 2.5 \tag{1}$$

Where k_{qf} = FSO; S_{bk} = characteristic effects which together stabilize the superstructure; S_{sk} = characteristic actions related to traffic load (including impact action) which overturn the superstructure.

For curved box-girder bridges, overturning resistance is computed in three steps. First, the location of the overturning axis is determined according to the layout of the bridge bearings. The overturning axis is a line connecting the last two effective bearings after a sequence of bearing failures under the traffic load as the bridge overturns around the axis. Second, based on the overturning axis, the effects of balanced actions and unbalanced ones are determined under various loads. Finally, FSO is determined by the ratio of those two sets of effects. To this effect, FSO can be defined according to the overturning axis, overturning moment, and overturning moment resistance.

According to Chinese code JTG D62-2012 (exposure draft) [22], the FSO for curved box-girder bridges is expressed as follows:

$$k_{\mathrm{qf}} = \frac{\sum F_{\mathrm{G}i} x_i}{(1+\mu)(q_{\mathrm{k}}\Omega + P_{\mathrm{k}})d} \tag{2}$$

Where q_{k} = uniform load in lane loads; P_{k} = concentrated load in lane loads; $F_{\mathrm{G}i}$ = every bearing reaction in a finished bridge; μ = impact coefficient; x_i = vertical distance from each bearing to the overturning axis; Ω = area enclosed by the overturning axis and lateral loading lane; d = the maximum vertical distance from the lateral loading lane to overturning axis.

3. Model setup

3.1. Project profile

To compute the FSO of curved box-birder bridges and to investigate the relevant influencing parameters, finite element models were built with different curvature radius and separately determined their overturning axes. The models were established using a portion of an existing overpass ramp as a prototype. The structures were concrete box-girder bridges with three-span length of 3 × 25 m and single-cell single-box sections. The middle piers were single column piers. Double torsional bearings were set at the two abutments with a central space of 2.6 m. The traffic load was Highway Grade I.

3.2. Model making

Model parameters: There are two parameters on FSO k_{qf}: curvature radius *R* and bearing eccentricity *e*. The values of outward *e* from the middle pier were: 0, 0.1, 0.2, 0.3, 0.4, and 0.5 m; *R* values were: 50, 100, 200, 300, 400, 500, 600, 700, 800, 900, and 1000 m. Altogether there were 6 × 11 = 66 models made according to these value ranges.

Section size: The height of girder was 1.8 m, the width of top slab was 8.8 m, the width of bottom slab was 4.1 m, the thickness of cantilever end was 0.2 m, and the root of cantilever was circularly connected. The section profile was shown in Figure 1.

Material characteristics: In superstructure the concrete grade C50 was applied, which modulus of elasticity $E = 3.45 \times 107$ kN/m^2, Poisson ratio $\mu_p = 0.2$, and density $\rho = 25$ kN/m^3.

Boundary conditions: Bearings were fixed in x and z directions and movable in the y direction. One middle pier was fixed and the abutments were torsion resistant.

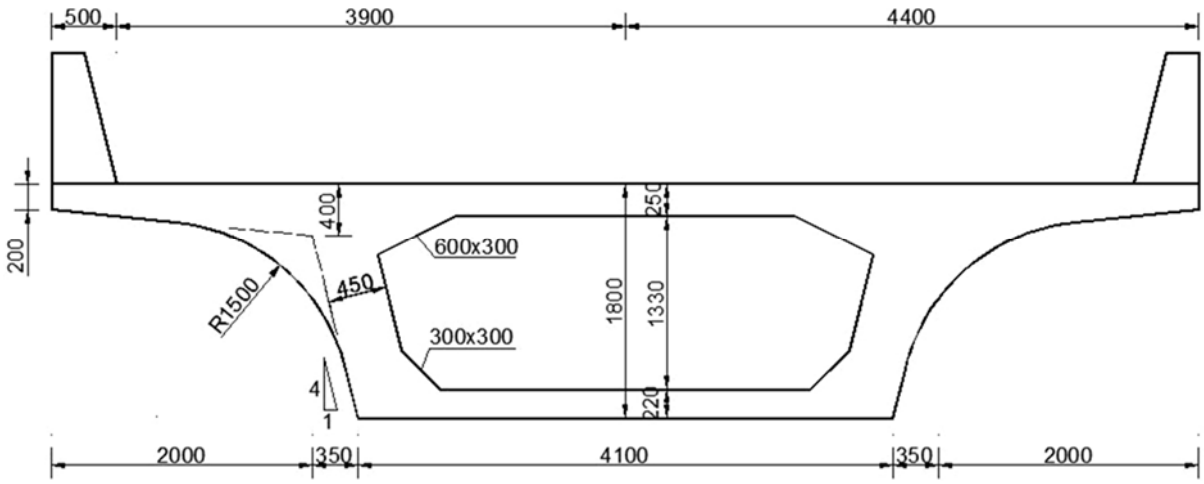

Figure 1. Section dimensions (mm)

Live loads: According to Chinese regulation (JTG D60-2015), two different grades of standard values of traffic load, Highway Grade I and Highway Grade II, are applied for different road design. Lane load is composed of uniform load and concentrated load shown in Figure 2.

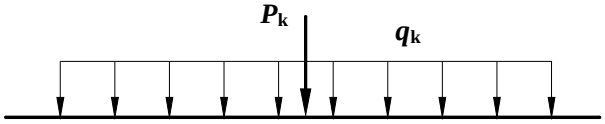

Figure 2. Lane load pattern

For Highway Grade I, the standard value of uniform load q_k = 10.5 kN/m, and concentrated load P_k is taken as Table 1. When calculating shear effect, the values of P_k will be multiplied by 1.2.

Table 1. Standard values of concentrated load for Highway Grade I

Concentrated load	Effective span l (m)		
	$l \leq 5$	$5 < l < 50$	$l \geq 50$
P_k(kN)	270	2(l+130)	360

To comprehensively determine the setup's stability against overturning, a plane load of Highway Grade I was imposed, 1.4 m from the lane axis to the crash barrier and 0.5 m from the outer vehicle wheel to the crash barrier. A vehicle load of Highway Grade I also was set for comparison with the loading type shown in Figure 3; this loading location was 0.5 m from the outer vehicle wheel to the crash barrier under the unfavourable conditions.

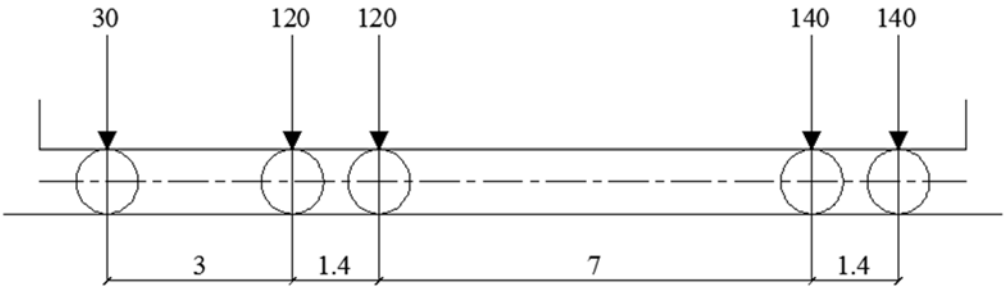

Figure 3. Vehicle loading layout (units: m, kN)

4. Influence factors of stability against overturning

As described in formula (2), seven factors influencek_{qf}. They were analysed in detail only for three equal-span curved box-girder bridges with single column piers.

1) Bridge span affects concentrated loadP_k, while the uniform load remains unchanged as q_k = 10.5 kN/m.

2) Once the bridge is complete, bearing reactions F_{Gi} are influenced by many factors including the superstructure type and weight, R, abutment bearing space, and e.

3) The vertical distance x_i is affected by the selection of axis, abutment bearing space, R and e, and other factors.

4) Several factors may influence the area Ω enclosed by the overturning axis and lateral loading lane, including the lane loading location, selection of overturning axis, bridge width, R, e, and bearing layout.

5) The maximum vertical distance d can be affected by the lane loading location, selection of overturning axis, bridge width, R, and e.

Generally, the structure dimensions of the bridge, self-weight, and bearing layout are the major factors influencing the structure's overturning resistance. Curvature radius R and bearing eccentricity e influence all the above parameters, resulting in complex influencing rules for k_{qf}. As mentioned above, R and e were specifically focused on for this reason.

4.1. Influence of curvature radius and bearing eccentricity on bearing reactions

4.1.1. Reactions under self-weight. The bearings were numbered as shown in Figure 4.

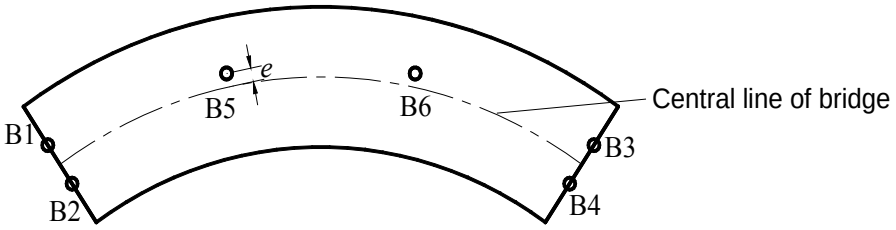

Figure 4. Bearing layout and numbering of a curved bridge

The structure was symmetrical, so reactions were symmetrically distributed under self-weight. Therefore, we only assessed reaction 1 F_{G1}, reaction 2 F_{G2}, and reaction 5 F_{G5}. Then the curves of these reactions versus R were drawn as shown in Figure 5 and the curves of the reactions versus e were drawn as shown in Figure 6.

If e is fixed, when R < 300 m, the influence of R on bearing reactions F_{Gi} is large; when R > 300 m, the influence of R on F_{Gi} is small (Figure 5). When F_{G1} increases, F_{G2} decreases and produces torque. Thus, bearing eccentricity e_{op} can be controlled to minimize torque according to the relationship between F_{G1} and F_{G2}.

Figure 5 (a) shows where as e = 0.5 m, F_{G1} decreases as R increases and even falls below zero, at which point F_{G1} provides tension and the bearing has been separated. In practice, of course, it is crucial to avoid bearing separation.

Figure 5(c) shows that when e = 0.1 m, F_{G5} changes very little as R varies. At e > 0.1 m, F_{G5} fluctuates considerably as R increases. These fluctuations have little impact on the whole reaction, however.

Figure 6 contains a similar linear trend between reactions and e when R is fixed. For B1 in Figure 6 (a), the trend is descending at almost the same negative slope. While for B2 in Figure 6 (b), the trend is ascending at almost the same positive slope. For B5 in Figure 6 (c), the lines descend at different negative slope; the reactions decrease faster as e increases when R is smaller, but this change does not significantly impact the reaction as a whole.

Reaction curves of models with R = 50 m were plotted as shown in Figure 7 to study the influence of e on reactions and determine the corresponding changing rules. As e increased, reaction 1 (outer side) decreased while reaction 2 (inner side) increased. The two curves intersect at about e = 0.355 m, which is the optimal eccentricity e_{op} at which point the torque distribution is uniform. Figure 7 also shows where reaction 5 did not markedly change, suggesting that e has little impact on reaction 5 (middle pier). The reaction of the middle pier was much larger than the reactions of the abutment, indicating that the middle pier performs an important load-bearing role.

At the optimal eccentricity e_{op} the reactions of the inner and outer sides are equal to each other. The e_{op} of bridges with different R values were calculated as shown in Table 2 and the curve of e_{op} versus R was plotted as shown in Figure 8. The curve fit to the following equation:

Table 2. Optimal eccentricity of bridges with different curvature radii (unit: m)

R /m	50	100	200	300	400	500	600	700	800	900	1000
e_{op}/m	0.355	0.153	0.074	0.049	0.037	0.029	0.024	0.021	0.018	0.016	0.015

$$e_{op} = 20.09R^{-1.05} \quad (3)$$

Equation (3) indicates that e_{op}decreases as R increases. When R < 300 m, e_{op} decreases especially dramatically; when R > 300 m e_{op} changes gradually.

4.1.2. Reactions under traffic load. Highway Grade I lane and traffic loads were imposed on the model bridges to check for bearing separation in the superstructure. A 55t intensive traffic team was deployed onto the superstructure as described in the exposure draft of JTG D62-2012 (the exposure draft) [22]. The minimum k_{qf} was raised to 2.5 from 1.3.

The results, curves, and relations of reactions with e and R under traffic load are similar to those under self-weight; the only point worth emphasizing is F_{G2}. Under the combined action of e and R, B2 began to separate and pressure changed into tension, as shown in Figure 9. This tension was quite large especially for bridges with small e and small R values.

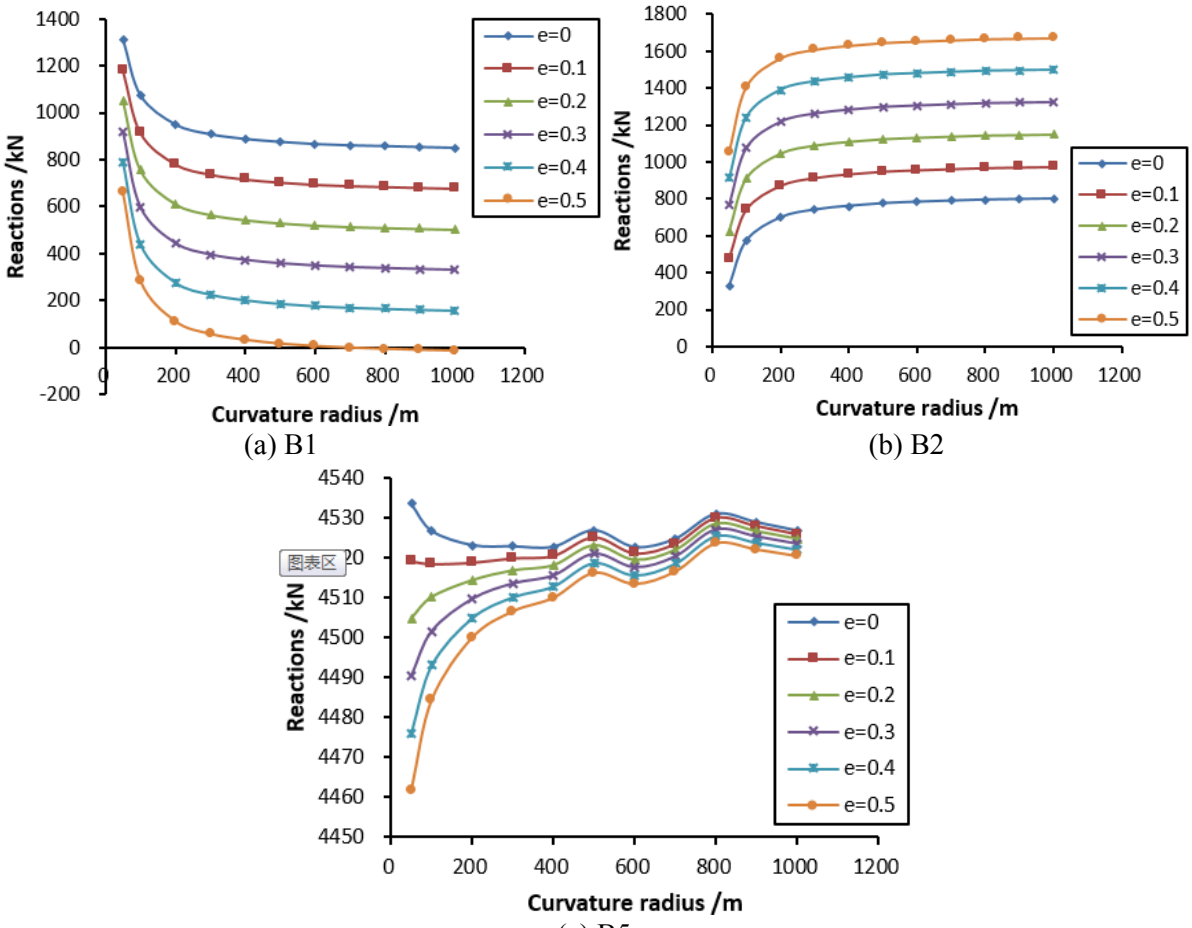

Figure 5. Curves of reactions versus curvature radius

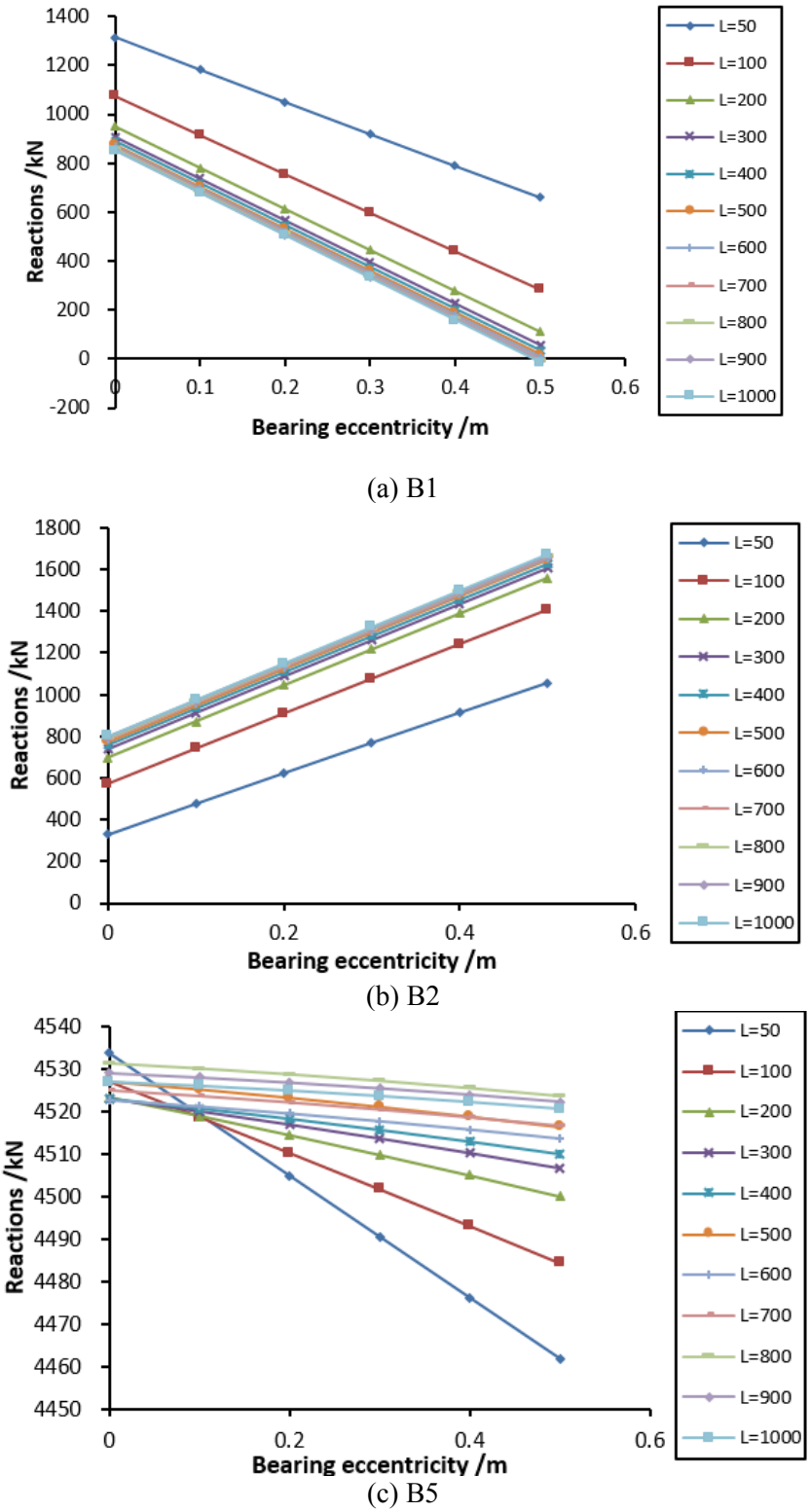

(a) B1

(b) B2

(c) B5

Figure 6. Curves of reactions versus bearing eccentricity

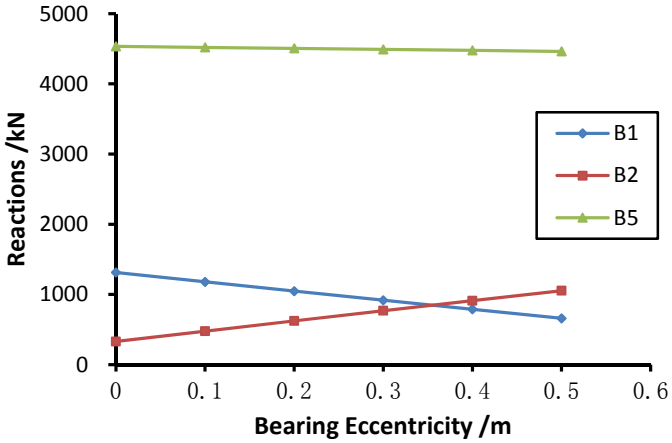

Figure 7. Reactions of bridges with curvature radius of 50 m

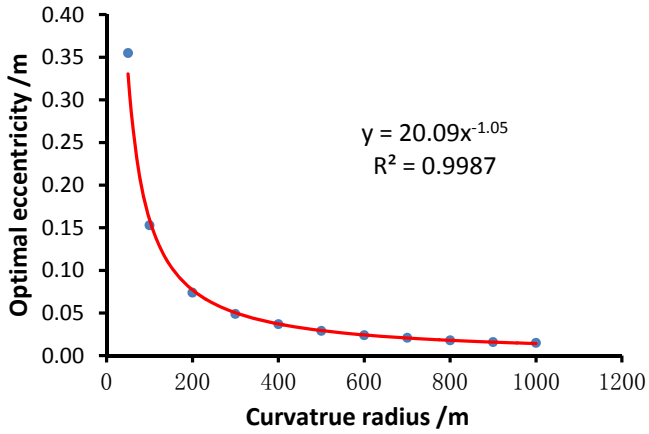

Figure 8. Relationship between optimal eccentricity and curvature radius under self-weight

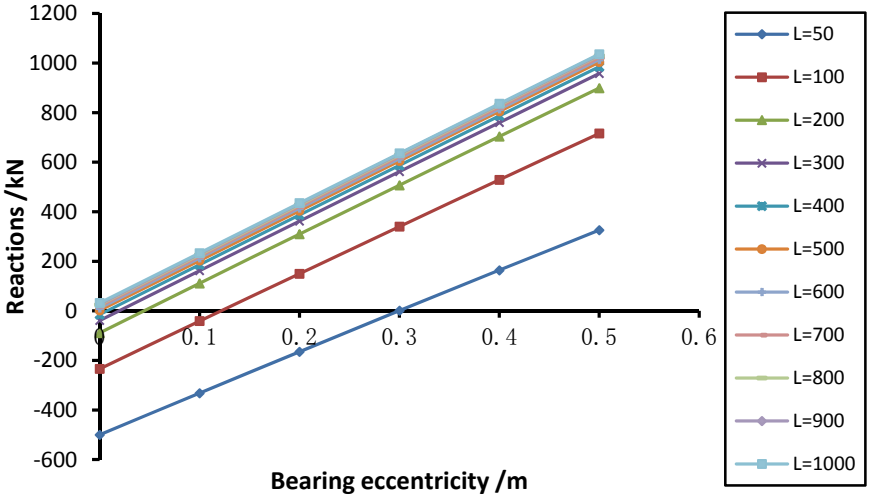

Figure 9. Curves of reactions versus bearing eccentricity for B2

The optimal eccentricities under traffic loads are almost the same as those under self-weight, so the relationship between e_{op} and R shown in equation (3) can also be applied under traffic loads.

4.2. Calculation of parameter varieties

According to equation (2), the parameters but $F_{\mathrm{G}i}$ can be computed to determine the values of k_{qf}.

4.2.1. Impact factor. The following impact factors were analysed as listed in Table 3. R influences the structural basic frequency to some extent, but the influence is scant and can be neglected when R > 200 m. When R < 200 m, the structural basic frequency and the impact factor increase as R increases.

Table 3. Impact factors of bridges with different curvature radii

R /m	50	100	200	300	400	500	600	700	800	900	1000
Structural basic frequency /Hz	4.63	4.77	4.80	4.81	4.81	4.80	4.81	4.81	4.80	4.80	4.80
k_{qf}	0.255	0.260	0.262	0.262	0.262	0.262	0.262	0.262	0.262	0.262	0.262

4.2.2. Vertical distances from bearings to overturning axes. The vertical distances x_i of our model bridges are shown in Figure 10. When R < 600 m, x_1 and x_2 decrease as R increases; they remain stable when R > 600 m. For B1, $x_1 \approx 0$ and for B2, $x_2 \approx 2.6$ m. For B5, x_5 is not zero when R > 600 m and increases as R increases, but decreases as e increases.

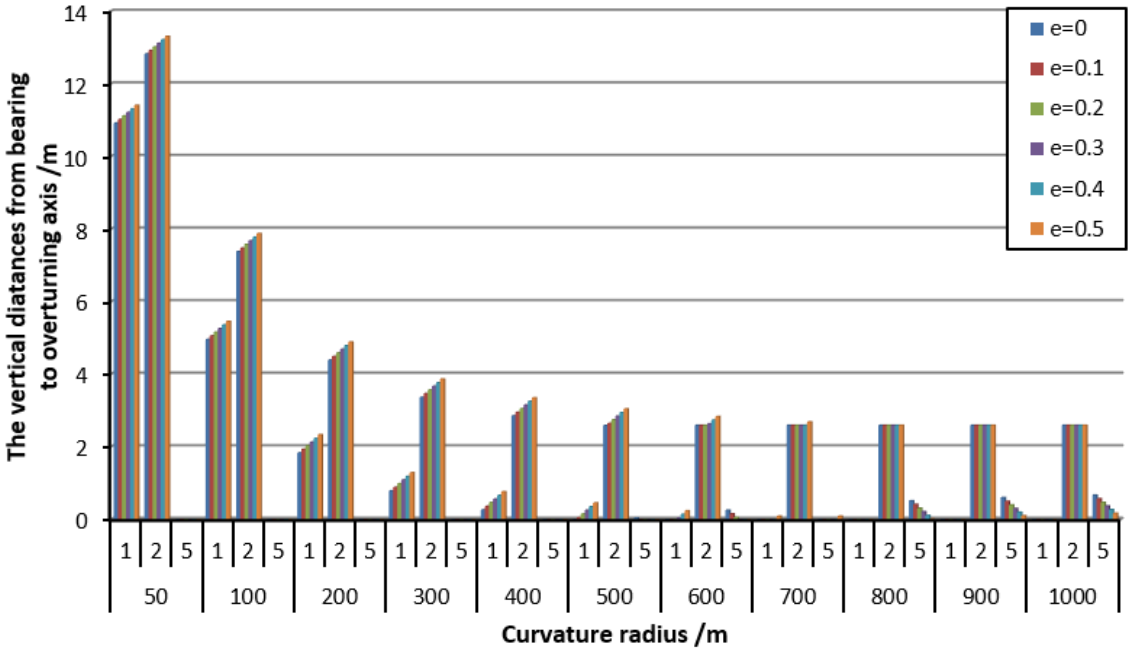

Figure 10. Vertical distances from bearings to overturning axes

The location of the overturning axis is fixed for bridges with R < 500 m or R > 700 m. (1-3) was defined to mean that the overturning axis is the connecting line of B1 to B3. For bridges with R < 500 m, the overturning axis is (5-6); for bridges with R > 700 m, the overturning axis is (1-3). Bridges with 500 m < R < 700 m have different overturning axes (see Table 4).

Table 4. Location of overturning axes for bridges with curvature radii of 500-700 m

R /m	*e* /m					
	0	0.1	0.2	0.3	0.4	0.5
500	1-3	5-6	5-6	5-6	5-6	5-6
600	1-3	1-3	1-3	5-6	5-6	5-6
700	1-3	1-3	1-3	1-3	1-3	5-6

4.2.3. Areas enclosed by overturning axis and lateral loading lane. The curves of areas Ω enclosed by overturning axis and lateral loading lane were plotted as shown in Figure 11. Generally speaking, Ω increases as R increases when R is initially smaller, and Ω decreases as e increases. Ω_{max} Converged on the same curve when R was sufficiently large, however, and was not influenced by e; this curve is expressed by equation (4) as shown in Figure 12.

$$\Omega_{\max} = 1476.2R^{-0.358} \quad (500\ \text{m} \le \text{R} \le 1000\ \text{m}) \tag{4}$$

4.2.4. Maximum vertical distance from lateral loading lane to overturning axis. The maximum vertical distance d from the lateral loading lane to overturning axis among our model bridges was analysed and plotted as shown in Figure 13. When the overturning axis is the connecting line of two pier bearings B5 and B6, d decreases as e increases; when the overturning axis is the connecting line of two outer abutment bearings B1 and B3, d is unchanged as e increases because the overturning axis location stays constant relative to the loading lane. Generally speaking, d decreases as R increases; it decreases slowly when 200 < R < 500 m and is entirely independent of e when R ≥ 800 m.

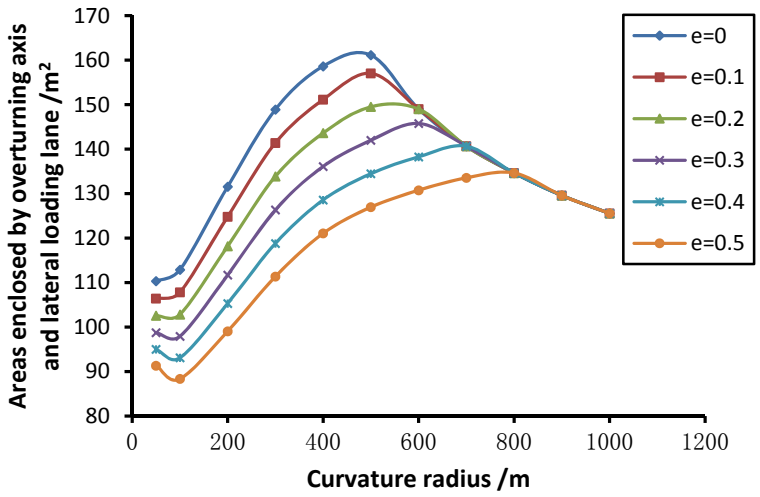

Figure 11. Areas enclosed by overturning axis and lateral loading lane

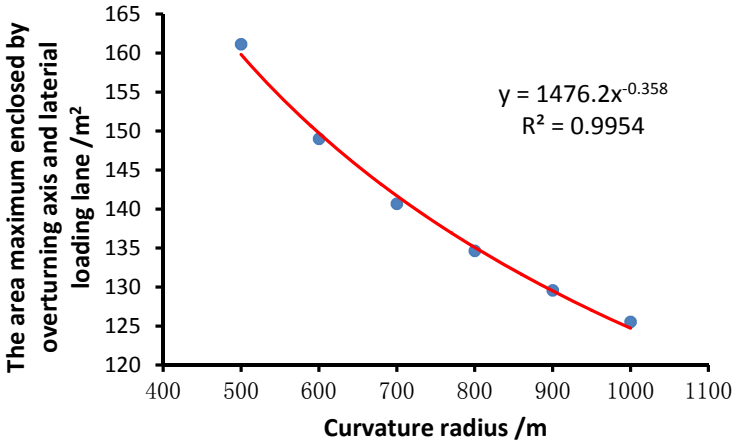

Figure 12. Maximum area enclosed by overturning axis and lateral loading lane

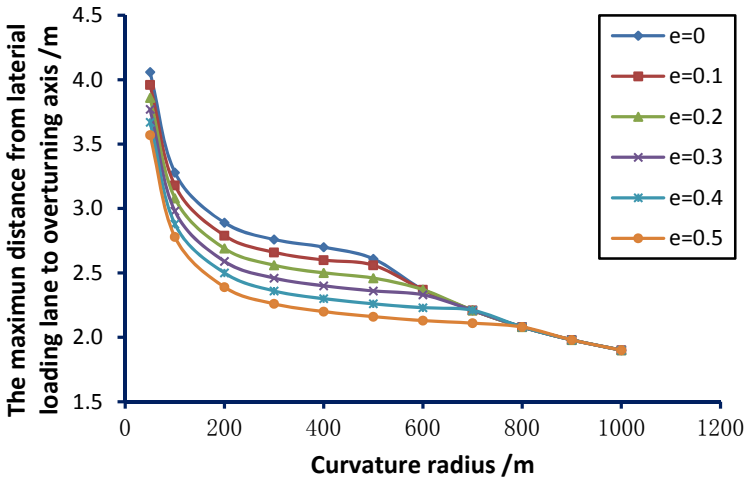

Figure 13. Maximum vertical distances from lateral loading lane to overturning axis

5. Resulting factors of stability against overturning

All the data described in Section 3 were plugged into equation (2) to compute k_{qf} considering the influence of *R* and *e*.

5.1. Comparison among factors of stability against overturning under lane loads and vehicle loads

The k_{qf} of bridges under lane loads and vehicle loads were plotted as the curves shown in Figure 14 and Figure 15, respectively. k_{qf} has the same varying trends under both types of loads, though it was slightly lower under lane loads on the whole. Per the relevant regulations, k_{qf} must be assessed under the unfavorable loads, we chose the smaller (lane) loads for analysis here, accordingly. In JTG D62-2012 (the exposure draft) [22], lane loads are also adopted to compute k_{qf} for superstructures and to check the integrated stability of bridges.

Our k_{qf} calculations are shown in Figure 14. The curves of k_{qf} can be divided into two parts. In the left-hand part, k_{qf} decreases as *R* increases and increases as *e* increases. In the right-hand part, k_{qf} increases as *R* increases, gradually stabilizes as *e* increases, and converges to a similar curve in the end. The convergence curve can be expressed as follows (Figure 16):

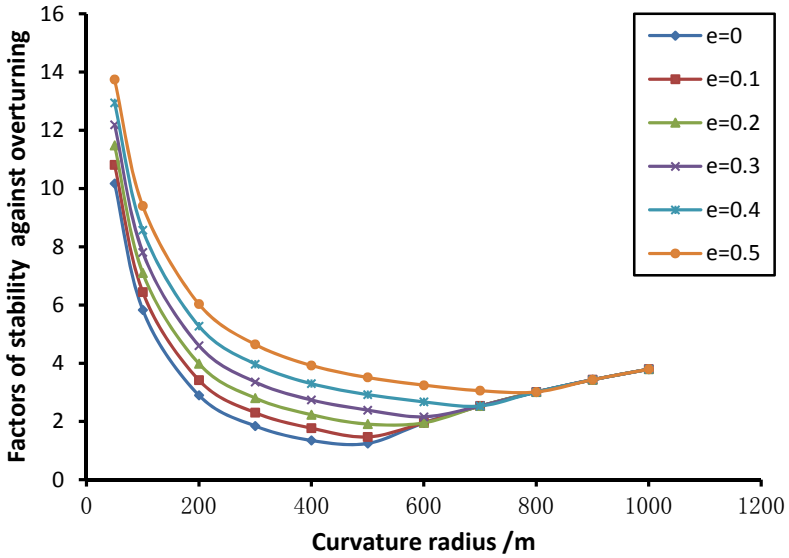

Figure 14. Factors of stability against overturning under lane loads

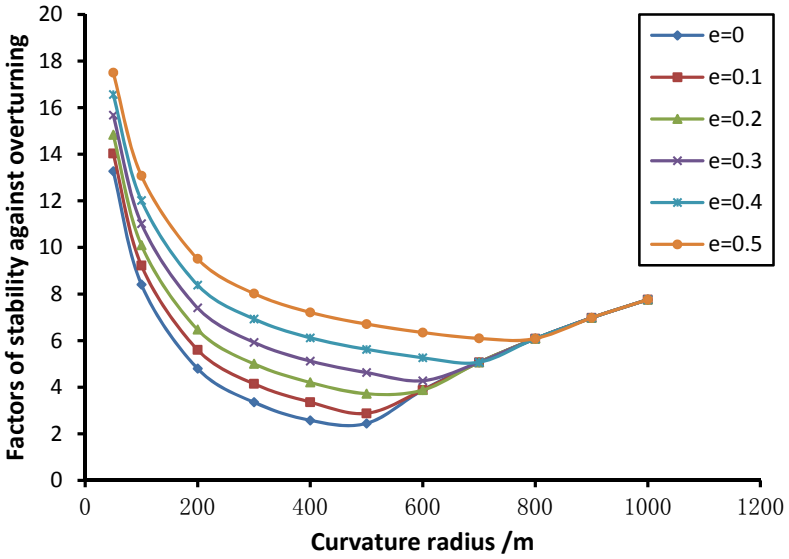

Figure 15. Factors of stability against overturning under vehicle loads

$$k_{\mathrm{qf,con}} = 3.6787\ln(R) - 21.591 \quad (500\ \mathrm{m} \le \mathrm{R} \le 1000\ \mathrm{m}) \tag{5}$$

When R > 700 m, k_{qf} does not vary with e. At this point, the overturning axis is located in the connecting line of the abutment outer bearings, so changes in e at the middle pier do not influence the overturning axis location, Ω area, and maximum vertical distance d (i.e., the denominator of equation (2)). The changes in e only influence the distance x_i. The decrease in reaction moment resulting from the middle pier bearings is almost equal to the increase in reaction moment resulting from the abutment inner bearings. As a result, changes in e have little influence on k_{qf} and k_{qf} remains effectually constant. There are similar symmetrical shapes in both Figure 11 and Figure 14. This suggests a negative correlation between k_{qf} and Ω, and indicates that Ω has significant effect on k_{qf}.

These observations altogether indicate that e has a substantial effect on k_{qf} with shorter R and less with longer R. Regardless of e value, k_{qf} decreases first and increases later as R increases.

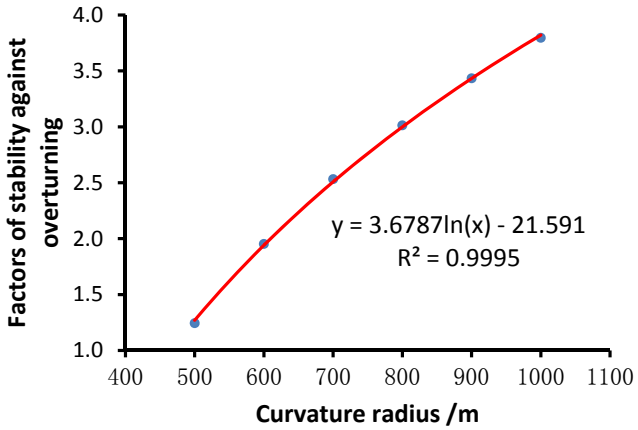

Figure 16. Convergence curve of factors of stability against overturning under lane loads

5.2. Factors of stability against overturning with optimal bearing eccentricity

Bridges with different R have different e_{op} values as listed in Table 2. We calculated the optimal k_{qf} via interpolation method according to e_{op} and plotted it as the curve shown in Figure 17.

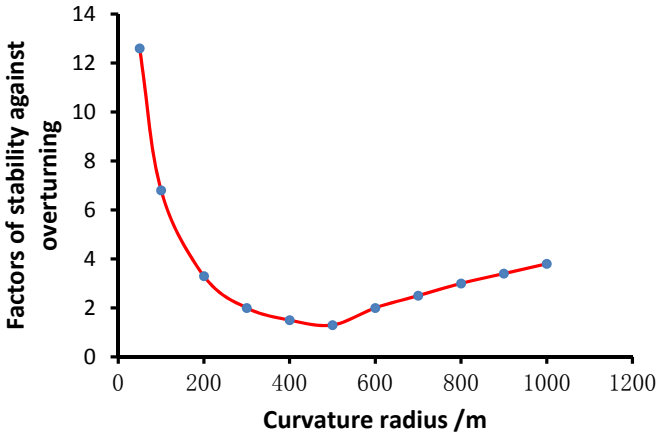

Figure 17. Factors of stability against overturning under optimal bearing eccentricities

Figure 17 indicates that if e_{op} is adopted, k_{qf} first decreases and later increases as R increases. It equals 500 m at the lowest point. When R < 500 m, k_{qf} decreases rapidly, in other words, R is the element primarily influencing k_{qf}. When R > 500 m, k_{qf} decreases gradually to the point that R is no longer the main influencing element. We believe the most important influencing element is the self-weight of the superstructure.

The curve of k_{qf} is concave with variations in R. There exists a specific R which results in the minimum k_{qf}. The exposure draft referenced above requires k_{qf} above 2.5 under a Highway Grade I lane load. Therefore, k_{qf} is below the standard for bridges with $300 \leq R \leq 600$ m. It is recommend that

priority be given to keeping R as far as possible from the valley point of k_{qf} to design bridges with effective overturning resistance.

6. Conclusion

This paper introduces the expression of k_{qf} for curved bridges and discusses our analysis of the effects of R and e on k_{qf} under self-weight and traffic loads. Other parameters are also discussed in detail above. The following conclusions were made regarding the change rules of k_{qf} as influenced by R and e.

1) Lane loads should be adopted to analyze the overturning resistance of curved bridges. k_{qf} must be computed considering the unfavorable loads with the lowest FSO under the lane load. JTG D62-2012 (the exposure draft) [22] also supports this recommendation.

2) Bearing eccentricity e has significant influence on inner and outer side reactions of the abutment bearings. The outer side reaction decreases and the inner side reaction increases as e increases. The optimal eccentricity e_{op} can ensure uniform torque distribution. e does not have any substantial impact on middle piers.

3) For the models in this study, k_{qf} decreases as e increases and is markedly affected when $R < 500$ m; but k_{qf} decreases first and then increases later as R increases, changes more gradually, and finally converges to the same curve when $R > 500$ m.

4) The k_{qf} curve for three equal-span curved bridges with single column piers is a concave shape with variations in R. There exists a specific R which results in minimal k_{qf}. The R values must be designed far from the valley point in this curve to design a bridge with effective overturning resistance.

Acknowledgments

This work was supported by the National Natural Science Foundation of China (U1304515). The authors would also like to thank anonymous reviewers for valuable comments and suggestions.

References

[1] X. M. Pan, L. S. Sun, and B. W. Ning, "Analysis of restraint reaction force characteristics of curved beam bridges under action of vertical load," *Bridge Construction*, vol. 2011, no. 3, pp. 26-30, 2011 (Chinese).

[2] A. B. Sarode and G. R. Vesmawala, "Parametric study of horizontally curved box girders for torsional behavior and stability," *International Refereed Journal of Engineering and Science (IRJES)*, vol. 3, no 2, pp. 50 - 55, 2014.

[3] G. Y. Huang, C. Q. Lan, and X. Lan, "Analysis on overturning of single pier bridge and reinforcement design method," *Applied Mechanics and Materials*, no. 105-107, pp. 1338-1341, 2012.

[4] W. B. Peng, F. Dai, and E. Taciroglu, "Research on mechanism of overturning failure for single column pier bridge," *Proceedings of the 2014 International Conference on Computing in Civil and Building Engineering, ASCE,* Orlando, Florida, June 23-25, pp. 1747-1754, 2014.

[5] W. Han, J. Wu, C. S. Cai, and S. Chen, "Characteristics and dynamic impact of overloaded extra heavy trucks on typical highway bridges," Journal of Bridge Engineering, vol. 20, no. 2, Article ID 05014011, p. 11, 2015.

[6] L. Deng, W. Wang, and Y. Yu, "State-of-the-art review on the causes and mechanisms of bridge collapse," Journal of Performance of Constructed Facilities, vol. 30, no. 2, Article ID 04015005, p. 13, 2016.

[7] E. E. Diaz, F. N. Moreno, and J. Mohammadi, "Investigation of common causes of bridge collapse in Colombia," Practice Periodical on Structural Design and Construction, vol. 14, no. 4, pp. 194–200, 2009.

[8] F. Y. Xu, M. J. Zhang, L. Wang, and J. R. Zhang, "Recent highway bridge collapses in China: review and discussion," Journal of Performance of Constructed Facilities, vol. 30, no. 5,

Article ID 04016030, 8 pages, 2016.
[9] W. Xiong, C. S. Cai, B. Kong, and J. Ye, "Overturning-collapse modeling and safety assessment for bridges supported by single column piers," Journal of Bridge Engineering, vol. 22, no. 11, Article ID 04017084, p. 13, 2017.
[10] P. D. Li and L. J. Ma, "Study of truck load for overturning resistance checking calculation of single-column-supported ramp bridge," *Bridge Construction*, vol. 42, no. 3, pp. 14-18, 2012 (Chinese).
[11] Y. C. Liu, "Analysis of pier girder consolidation single column pier bridge overturning and reinforcement design method," *Transportation Science & Technology*, vol. 260, no. 5, pp. 43-45, 2013 (Chinese).
[12] X. F. Yin, X. W. Yang, J. M. Feng, and L. Li, "Factor analysis on stability against overturning of curved continuous bridges with single column piers," *Highways & Automotive Applications*, vol. 172, no. 1, pp. 156-161, 2016 (Chinese).
[13] J. Zhang, and W. J. Xiao, "The research of single column pier bridge performance against overturning," *Highway Engineering*, vol. 38, no. 4, pp. 170-173, 2013 (Chinese).
[14] *Code for Design of Highway Reinforced Concrete and Prestressed Concrete Bridges and Culverts*, Industry standard of China, JTG D62-2004.
[15] *Guide Highway Bridges Specifications, American Association of Official: AASHTO*, American Association of Official, AASHTO, 2003.
[16] *Steel, Concrete and Composite Bridge*, British Standard Institution BS5400: ptl-4: 1978.
[17] *General Specifcations for Design of Highway Bridges and Culverts*, Industry standard of China, JTG D60-2015.
[18] W. B. Peng, W. T. Xu, G. J. Chen, and F. Y. Lu, "Calculation method for anti-overturning capacity of single column pier girder bridge," *China Journal of Highway and Transport*, vol. 28, no. 3, pp. 66-72, 2015 (Chinese).
[19] F. Liang, "Study on overturning resistance of curved three-span girder bridges with single piers," *Highway*, no. 10, pp. 40-43, 2009 (Chinese).
[20] S. D. Lu, W. Xiong, X. D. Ding, J. S. Ye, and Z. G. Wei, "Influence of structure arrangement on anti-overturn performance of curved beam bridge with single-column piers," *Journal of Highway and Transportation Research and Development*, vol. 34, no. 5, pp. 95-101, 2017 (Chinese).
[21] J. F. Wang, Z. Y. Xu, X. L. Fan, and J. P. Lin, "Thermal effects on curved steel box girder bridges and their countermeasures," *Journal of Performance of Constructed Facilities, ASCE*, vol. 31, no. 2, Article ID: 04016091, p. 12, 2017.
[22] *Code for Design of Highway Reinforced Concrete and Prestressed Concrete Bridges and Culverts (the Exposure Draft)*, Industry standard of China, JTG D62 - 2012.
[23] G. H. Song, D. L. Che, and M. H. Li, "Overturning axis selection in curved box-girder bridges with single-column piers," *Mathematical Problems in Engineering*, Vol. 2018, Article ID 9206138, p. 9, 2018.